Study of Interactions Between Cells and Microbubbles in High Speed Centrifugation Field for Biomolecule Delivery

Chuan He[1] and Jie Chen[1,2]
[1]Department of Biomedical Engineering, University of Alberta, Alberta T6G 2V4, Canada
[2]Canadian National Research Council / National Institute for Nanotechnology, Alberta T6G 2M9, Canada
Emails: jc65@ualberta.ca

***Abstract* – Biomolecule delivery has a very wide range of applications in biology and medicine. In this study, a microbubble based delivery method was developed. In a high centrifugation field, cells deform and collide with microbubbles to induce intracellular pathways on cell membranes. As a result, biomaterials can then easily enter cells. Experimental results show that this delivery method can achieve high delivery efficiency. Simulation results showed that cells with more deformed structure experienced higher strain on cell membranes than cells with less deformed structure. The models can help explain how centrifugation affects cell membrane permeability. By controlling cell morphology and its mechanical properties, high biomolecule delivery efficiency can be achieved.**

Keywords – Cell membrane permeability, centrifugation, microbubbles, ANSYS, membrane deformation, localized permeability increase.

I. Introduction

Cells usually uptake selective extracellular materials. The central theme of various delivery methods is to bypass cell membranes and inject foreign biomaterials into cells with minimum cell damage. One approach to increase cell membrane permeability is by using viruses: a technique which is still the most efficient to date. However, a practitioner cannot fully control the virus after injecting it into a human body. Although a virus is programmed to target non-functional cells, it might still attack healthy cells, thus leading to unexpected lethal diseases. Researchers have been aware of the virus safety issue for a long time, and alternative non-viral delivery methods have been developed.

Based on a literature study, non-viral methods can be generally divided into two categories: chemical-based methods and physical-based methods.

- Chemical carriers capsulize biomolecules such as DNAs inside the hydrophobic or hydrophilic regions in nano or micro scale size [1]. Such a special structure would induce the endocytosis of a cell. However, the sensitivity of different cells to different chemical carriers also varies greatly.
- Physical-based methods utilize temporary physical stimulation on the cell membrane to create intracellular pathways into the cell cytoplasm. The reported methods include electroporation, laser beam gene transduction, sonoporation, gene gun and liquid jet injection [2].

We developed a new physical-based delivery method which utilize microbubbles and high centrifugation field to increase cell membrane permeability [3,4]. This article is to further study the interaction between microbubbles and cells in a high centrifugation field. The article is organized as follows. The experimental results will be presented in Section II, and the delivery mechanism will be studied in Section III. The article concludes in Section IV.

II. Experimental Study

II.1 Preparing Microbubbles and Cells

The preparation of microbubbles and cells could be referred from previous work [4]. In short, the MCF-7 cells were harvested at a concentration of 50×10^4 cells/mL in each 1.5mL centrifuge tube. 15μL 5mg/mL FD (40kDa) solution (FD40S, Sigma-Aldrich) or 15μL 2.5mg/mL FD (70kDa) and the microbubble solution were in turn added to the cell suspension individually. The influences of microbubbles on cell membrane permeability were studied at various centrifuge speeds (expressed in relative centrifugal force (RCF)) and volumes of microbubble solution. The cell mixture was centrifuged at 4ºC with the designed parameters (Allegra™ 25R centrifuge, rotator: TA-15-1.5, Beckman Coulter). The range of the centrifuge speeds and volumes of microbubble solution were 28g (500RPM) to 2795g (5000RPM) and 5 to 85μL, respectively. The delivery efficiency was performed on FACS analysis and the cell viability was analyzed by MTT assay.

II.2 Result Analysis

Fig. 1 shows a typical Fluorescence Activated Cell Sorting (FACS) diagram of MCF-7 cells after delivering with FD40kDa and FD70kDa. Based on the results, MCF-7 cells centrifuged alone show a very low fluorescent background, while the sample centrifuged with the fluorescent material shows a slight shift to the right, possibly because some of the FD40kDa or FD70kDa attached onto the MCF-7 cell

surfaces. For the sample centrifuged with microbubbles, MCF-7 cells present a very strong fluorescent signal, and the peak of the fluorescence curve shifts greatly to the right. Fig. 2 shows the delivery efficiency and cell viability of MCF-7 cells under varied centrifugation speeds and volumes of microbubble solution. During the evaluation of the effect of the centrifugation speed, the volume of the microbubble solution was set at 45μL. The delivery efficiency shows an increasing trend as the centrifugation speed increases. However, for the samples delivered with FD70kDa (the blue

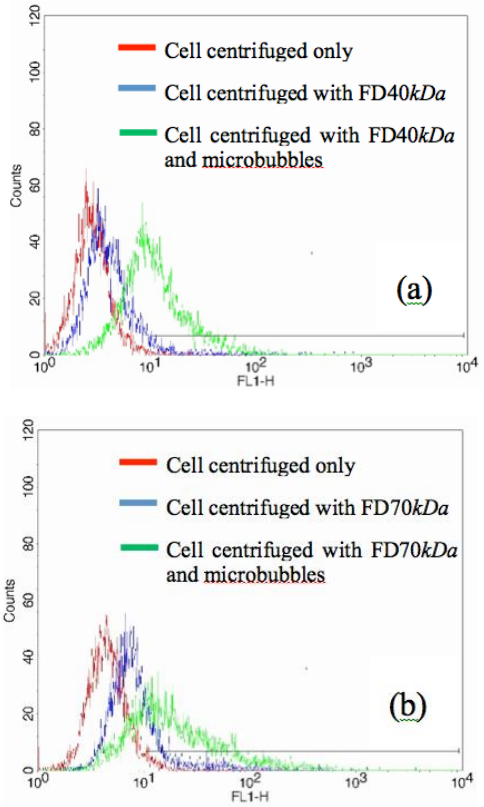

Figure 1: A typical FACS diagram of MCF-7 cells: (a) the red curve stands for MCF-7 cells centrifuged alone. The blue curve stands for MCF-7 cells centrifuged with FD40kDa, while the green curve stands for MCF-7 cells centrifuged with FD40kDa and microbubbles; (b) the red curve stands for MCF-7 cells centrifuged alone. The blue curve stands for MCF-7 cells centrifuged with FD70kDa, while the green curve stands for MCF-7 cells centrifuged with FD70kDa and microbubbles.

curve), the absolute value of the delivery efficiency is always smaller than that of the samples treated with FD40kDa (the red curve). The cell viability is shown by the green bar. The cell viability values drop significantly when the centrifugation speed increases to 1006g (3000RPM). There is no significant difference for the cell viabilities obtained when treated above 1006g (3000RPM) (Fig. 2a). To investigate the effect of the volume of microbubble solution, the centrifugation speed was set at 1006g (3000RPM). As shown in Fig. 2b, the delivery efficiency can also be increased by increasing the volume of the microbubble solution. The delivery efficiency of the samples treated with FD70kDa (the blue curve) is still lower than that of the samples treated with FD40kDa (red curve) and fluctuates around 45% as the volume of the microbubble solution increases. The cell viability (the green bar) exhibits a decreasing trend as the volume of the microbubble solution increases. The lowest cell viability is only 3.5% when 85μL microbubble solution is treated with the sample.

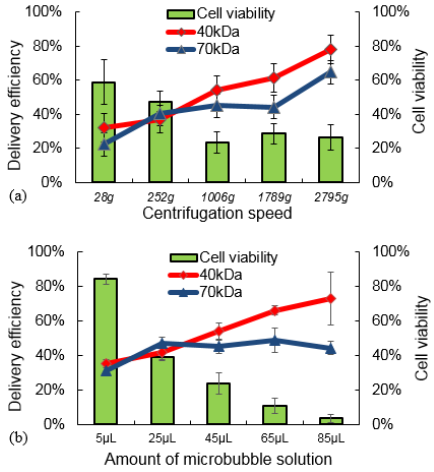

Figure 2: FD delivery efficiency and cell viability of MCF-7 cells: (a) delivery efficiency of FD (red curve: 40kDa, blue curve: 70kDa) and cell viability of MCF-7 cells at different centrifugation speeds; (b) delivery efficiency of FD (red curve: 40kDa, blue curve: 70kDa) and cell viability of MCF-7 cells with different volumes of microbubble solution.

III. Mechanism Study

III.1 Important Factors to Be Considered

There are three important factors to be considered in the mechanism study (1) collisions between microbubbles and cells; (2) microbubble bursting; and (3) change in cell morphology.

- Collisions between microbubbles and cells: This is due to the opposing direction of movement between microbubbles and cells in high-speed centrifugation fields. The liquid between the microbubbles and the outer layer of cell membranes is squeezed and thus induces a hydrodynamic force on the cell membrane [5]. This force can break the cell membrane especially near the collision region. However, the Derjaguin-Landau-Verwey-Overbeek (DLVO) force and membrane undulation force provide a repulsive force to impede the microbubble's collision with cells. Therefore, there is a critical velocity for membrane penetration to happen. Since this effect is mainly due to collision, this force is named "collision induced impulsion" (CII).
- Microbubble bursting is the second proposed mechanism. Microbubbles might burst due to the collision between a

microbubble and a cell, a microbubble and another microbubble, or a microbubble and the side-wall of the centrifuge tube. Microbubble bursting will lead to a similar situation as that in microbubbles-assisted sonoporation.

- Cell morphology is also a key element which determines the responses of cell membrane permeability to external forces. In our proposed method, a cell experiences a highly deformed state. Hoffman and Inoue centrifuged cells under conditions similar to those in our experiments, using a high speed camera to observe cell morphology change at high centrifugation speeds [6]. Although these shape changes are reversible for most cells, cells with special morphologies during the centrifugation process are of interest in this study. Investigating the interaction between microbubbles and deformed cells is critical for understanding the role of centrifugation and microbubbles during the process.

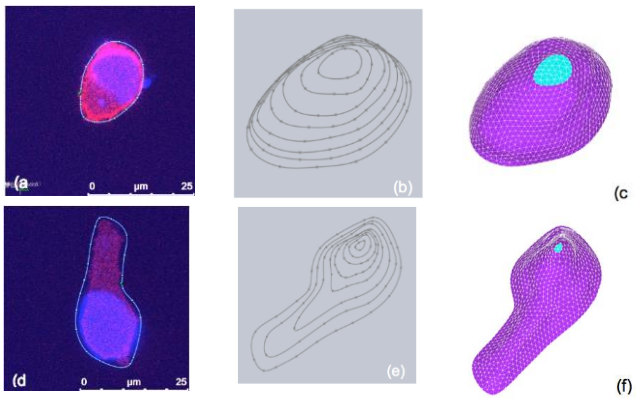

Figure 3: Operation processes for reconstructing deformation type I and deformation type II cells: (a) and (d) confocal microscope images from our lab, the contours are drawn on the image to define the cell boundary; (b) and (e) a stack of boundary contours, these contours were used to generate the cell membrane; (c) and (f) cell models after meshing in ANSYS®

III.2 Building Finite Element Models

To rebuild the cell morphology, Dailey and Gefen developed a new method using confocal microscope images to construct three- dimensional finite element models for in-vitro cell morphologies and analyzed cell mechanics by using these models [7]. In this study, the same method was used to build two deformed cells under the centrifugation field. The z-stack images we obtained were transferred to CAD software SolidWorks2012. First, parallel planes with an interval of 0.4μm were created at different heights, and then each image was inserted onto the plane following the sequence. Since most microbubble collisions happen on the cell surface facing the liquid, only the images of the upside body of the cells were selected for the model building. After inserting the image onto the corresponding plane, the contours of the cell membrane were manually drawn on each image, as shown in Fig. 3a and 3d. The cell membrane surface was then formed by lofting the spline contours onto different planes as shown in Fig. 3b and 3e.

The rebuilt cell morphology models were transferred to ANSYS® to generate finite element models. Both the deformation type I and deformation type II cells were meshed with four-node tetrahedral isotropic solid elements (node 285) for the cell body and three-dimensional four nodes shell elements (node 181) for the cell membrane. The deformation type I cell model had 19417 elements in the cell solid and 2641 elements in the cell membrane. The deformation type II cell model had 11364 elements in the cell solid and 2690 elements in the cell membrane. The cell models after the meshing process are shown in Fig. 3c and 3f.

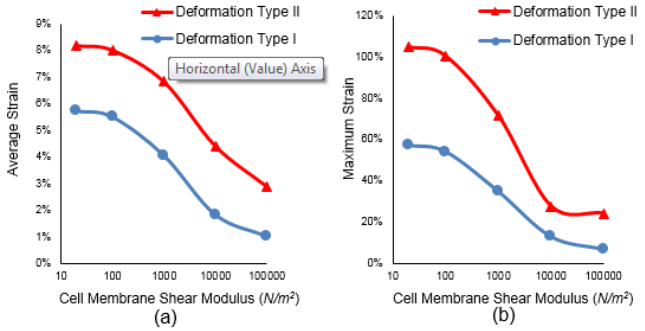

Figure 4 (a) average strain on cell membrane of deformation type I and deformation type II cell by varying cell membrane shear modulus $G_{membrane}$; (b) maximum strain on cell membrane of deformation type I and deformation type II cell by varying cell membrane shear modulus $G_{membrane}$.

III.3 Theoretical Results

For the results calculated in this study, the cell is modeled as an elastic body based on continuum mechanics theory. An estimated hydrodynamic pressure of $1.73 \times 10^5 \mathrm{N/m^2}$ was applied through the cell surface. Cell membrane permeability was evaluated based on the equivalent strain or Von Mises strain on the membrane. The equivalent strain could be obtained using the following equation

$$\varepsilon_e = \frac{1}{1+\nu}\left\{\frac{1}{2}\left[(\varepsilon_1-\varepsilon_2)^2+(\varepsilon_2-\varepsilon_3)^2+(\varepsilon_3-\varepsilon_1)^2\right]\right\}^{1/2}$$

where ε_1,ε_2 and ε_3 are the principal strains from the ANSYS® calculation results and ν is the pre-set Poisson's ratio. The comparison was made by varying the cell membrane shear modulus $G_{membrane}$ on the two deformed cell. Fig. 4 shows the average and maximum strain on the cell membrane as $G_{membrane}$ increases. By increasing $G_{membrane}$, both the average strain and maximum strain in the two deformed types of cells are decreased. The deformation type II cell undergoes a general 2% larger average strain than the deformation type I cell under all the $G_{membrane}$ tested. Fig. 4b presents the results

of the maximum strain on the cell membrane of both types of deformed cells. Overall, the maximum strain decreases as $G_{membrane}$ increases. The maximum strain on deformation type II cell is always higher than the one on deformation type I cell especially in the low $G_{membrane}$ region.

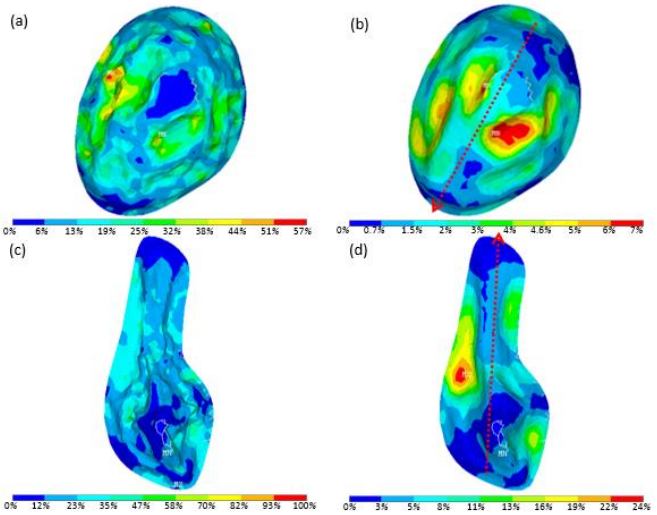

Figure 5 (a) equivalent strain distribution on the cell membrane of deformation type I cell when $G_{membrane}$ =20N/m^2; (b) equivalent strain on the cell membrane of deformation type I cell when $G_{membrane}$=10^{5}N/m^2; (c) equivalent strain on the cell membrane of deformation type II cell when $G_{membrane}$=20N/m^2; (d) equivalent strain on the cell membrane of deformation type II cell when $G_{membrane}$ =10^{5}N/m^2

The changing of equivalent strain distribution on the cell membrane by varing the cell membrane shear modulus $G_{membrane}$ is shown in Fig.5. Fig.5a and 5b present the equivalent strain distribution on the cell membrane of the deformation type I cell when $G_{membrane}$ is 20N/m^2 and 10^{5}N/m^2. The same condition was applied to the deformation type II cell, and the results are shown in Fig. 5c and 5d. Generally, the equivalent strain intensive area decreases as the membrane shear modulus $G_{membrane}$ increases. This result is rational, because increasing the $G_{membrane}$ increases the cell's ability to resist the shear force. Interestingly, when the membrane shear modulus $G_{membrane}$ is high, the equivalent strain intensive area is not only greatly minimized, but also tends to be localized in the cell elongation region. As shown in Fig. 5b, for the deformation type I cell, the direction of the elongation is towards the bottom-left corner (pointed out by axis). The high equivalent strain areas are almost axissymmetric with the axis and located on the side-wall of the cell. This phenomenon is even more obvious on the deformation type II cell. The elongation effect gives the cell a spindle morphology. As a result, a relatively thin and long region is formed. Fig. 5d reveals that, starting from the spindle-shaped head and extending toward the spindel-shaped tail, a major part of the high equivalent strain areas is located on the two sides of axis z (cell elongation direction). These results reveal that under the same CII pressure, both sides of the cell elongaion region are more fragile than the other regions on the cell membrane.

IV. CONCLUSION

In this article, a microbubble-based biomolecule delivery method was developed to increase cell membrane permeability in a high centrifugation field. The effects of cell deformed morphology and mechanical properties on cell membrane permeability were investigated. The structural behaviors of cells that were deformed to different degrees, such as deformation type I cells and deformation type II cells, were compared. The results indicated that both cell morphology and cell mechanical properties played an important role in the range of the strain values and strain distributions on the cell membrane. Generally, under the same CII pressure, cells with more deformed morphology experienced a higher strain than less deformed cells. This result was supported by the experimental data, which showed that a higher centrifugation field resulted in higher intracellular delivery efficiency.

Acknowledgement: The co-authors would like to acknowledge the funding support from Alberta Innovates Bio-Solutions, Canada.

References:

[1] Blanco, E., et al., Nanomedicine in cancer therapy: innovative trends and prospects. Cancer Sci, 2011. 102(7): p. 1247-52.

[2] Taira, K., K. Kataoka, and T. Niidome, Non-viral gene therapy gene design and delivery, 2005, Springer: Tokyo ; New York. p. xii, 487 p.

[3] He, C., et al., Biomolecule delivery into canola protoplasts by centrifuging cells with microbubbles. Febs Letters, 2013. 587(3): p. 285-290.

[4] He, C., et al, Microbubble-enhanced cell membrane permeability in high gravity field. Cellular and Molecular Bioengineering, 2013. 6(3), p. 266-278

[5] Chan, D.Y.C. and R.G. Horn, The Drainage of Thin Liquid-Films between Solid-Surfaces. Journal of Chemical Physics, 1985. 83(10): p. 5311-5324.

[6] Hoffman, J.F. and S. Inoue, Directly observed reversible shape changes and hemoglobin stratification during centrifugation of human and Amphiuma red blood cells. Proceedings of the National Academy of Sciences of the United States of America, 2006. 103(8): p. 2971-2976.

[7] Dailey, H.L., et al., Image-based finite element modeling of alveolar epithelial cell injury during airway reopening. Journal of Applied Physiology, 2009. 106(1): p. 221-232.